Radon-Wavelet Based Novel Image Descriptor for Mammogram Mass Classification

Submitted: 20th October 2018; accepted: 2nd June 2020

Sk Md Obaidullah, Sajib Ahmed, Teresa Gonçalves, Luís Rato

DOI: 10.14313/JAMRIS/2-2020/22

Abstract:

Mammography based breast cancer screening is very popular because of its lower costing and readily availability. For automated classification of mammogram images as benign or malignant machine learning techniques are involved. In this paper, a novel image descriptor which is based on the idea of Radon and Wavelet transform is proposed. This method is quite efficient as it performs well without any clinical information. Performance of the method is evaluated using six different classifiers namely: Bayesian network (BN), Linear discriminant analysis (LDA), Logistic, Support vector machine (SVM), Multilayer perceptron (MLP) and Random Forest (RF) to choose the best performer. Considering the present experimental framework, we found, in terms of area under the ROC curve (AUC), the proposed image descriptor outperforms, upto some extent, previous reported experiments using histogram based hand-crafted methods, namely Histogram of Oriented Gradient (HOG) and Histogram of Gradient Divergence (HGD) and also Convolution Neural Network (CNN). Our experimental results show the highest AUC value of 0.986, when using only the carniocaudal (CC) view compared to when using only the mediolateral oblique (MLO) (0.738) or combining both views (0.838). These results thus proves the effectiveness of CC view over MLO for better mammogram mass classification.

Keywords: *Image descriptor, radon transform, mammography, breast cancer, classification*

1. Introduction

Breast Cancer is the most frequent cancer among women, impacting over 1.5 million women each year and is also the cause of the highest number of cancer related death among women. In 2015, 570,000 women died from breast cancer – which is approximately 15% of all cancer deaths among women [1]. If breast cancer is early detected, it is one of the most treatable types of cancer. The primary imaging modality for breast cancer is done by a low cost X-Ray based technique which is known as mammography. Based on the processing modalities, mammography can be classified into two types: (i) Screen Film Mammography (SFM) and (i) Full Field Digital Mammography (FFDM). For SFM, images are captured on the film, whereas for FFDM, images are directly stored in the digital computer. As per the reported study in literature [2, 3], both type of mammography, have almost equal ability to detect suspicious lesions in the breast. The present work deals with the SFM images which are available through the BCDR-F03 dataset [4,5], one of the latest breast imaging film mammography benchmark datasets.

In recent years many computational approaches have been proposed for computer assisted diagnostic of breast cancer; these methods are known as Computer Aided Diagnostic methods or, in short, CAD [6]. A double checking procedure by radiologists is normally used to reduce the number of false-negative cases, but this has an obvious cost associated as the number of radiologists are not in general adequate in our health centres. Alternatively, a CAD system can help one radiologist to verify her/his observations with the result of the automated system without requiring another radiologist in the same place. That is why the importance of developing CAD system is in demand.

Presently various CAD systems have been proposed in the literature. The general framework for a traditional CAD system consists of three parts: (i) preprocessing the mammogram images for ROI extraction, (ii) feature extraction and finally (iii) classification. Recently, deep learning based approaches are also reported in literature which replaces the extraction of handcrafted features by combining step (ii) and (iii) in a single stage. In literature works are reported where image descriptors are combined with clinical information for better classification accuracy [6]. The present work focuses on an image descriptor based classification of masses from mammogram images. We have not considered any clinical information.

Among the reported image descriptors, Constantinidis et al. [7] and Belkasim et al. [8] considered the Zernike moment based descriptor to classify masses; texture based classification of calcification and masses using Haralick features [9] was reported by different authors [10–14]. Haralick texture features were employed in other areas of medical imaging also [15] and a comparison of texture features and a deep learning approach is reported in [16]. Wavelet [17, 18] and curvelet [19] analysis based feature descriptors are also used by different authors and combination of intensity and texture descriptors was explored by Ramos et al. [20]. Histogram of oriented gradient (HOG) based features was employed along with the clinical information for mammogram image classification by Moura and Guevara [6] and Arevalo et al. [5] used a convolution neural network to separate malignant and benign masses without using any clinical information reporting the effectiveness of a deep learning based approach over the traditional hand-crafted one.

In this paper, we propose a novel image descrip-

tor based on radon transform over multi-resolution images. The block diagram of the proposed method is shown in Figure 1. First film mammogram dataset is considered and images are categorized based on CC and MLO views; ROI are then extracted and their contrast is enhanced; next step computes a feature vector, followed by classification and performance comparison of multiple classifiers.

The rest of the paper is organized as follows: the contributions are reported in Section 2 where we discuss about the proposed image descriptor and the design of classifiers; experimental details are reported in Section 3, which include dataset description, experimental setup and results with a comparative study. Finally we conclude the paper in Section 4.

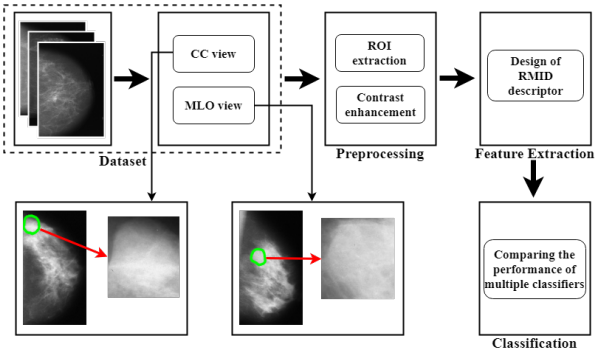

Fig. 1. Block diagram of the proposed method

2. Contribution Outline

As mentioned earlier, we propose a novel feature descriptor for classification of mammogram masses. In particular, our target is to classify malignant and benign masses from mammogram images using this novel image descriptor. We describe the image descriptor in detail in the following sub section.

2.1. Design of the Image Descriptor

The propose image descriptor uses the concepts of radon transform and multi-resolution analysis. In general, the radon transform is an integral transform computes the projection of an image matrix along a specified angle. This method has wide application in the domain of medical imaging as it is used to reconstruct images from medical CT scans. The radon transform method was introduced in 1917 by Johann Radon [21] and a formula for the inverse transform was also provided by him. The basic principal of these techniques are described below.

Radon transform. Radon transform is an integral transform that consists of a set of projections of a pattern at different angles [21], as illustrated in Figure 2 where, the part (a) shows the projection principal and part (b) shows different angles considered for the present work. It is a mapping of a function $f(x, y)$ to another function $fR(x, y)$ defined on the 2D space of lines in the plane, whose value at a particular line is equal to the line integral of the function over that line for the given set of angles. In other words, the radon transform of a pattern $f(x, y)$ and for a given set of angles may be assumed as the projection of all non-zero points. The projection output is the sum of the non-zero points for the image pattern in each direction (angle between 0 to π). Finally it results forming a matrix. The matrix elements are related to the integral of $f(x, y)$ over a line $Lin(\rho, \theta)$ defined by $\rho = x\cos\theta + y\sin\theta$ and can formally be expressed as

$$fR(\rho,\theta) = \int_{-\infty}^{\infty}\int_{-\infty}^{\infty} f(x,y)\delta(x\cos\theta + y\sin\theta - \rho)dxdy$$

where $\delta(.)$ is the Dirac delta function, $\delta(x) = 1$, if $x = 0$ and 0 otherwise. Also, $\theta \in [0, \pi]$ and $\rho \in]-\infty, \infty[$. For the radon transform, Lin_i be in normal form (ρ_i, θ_i).

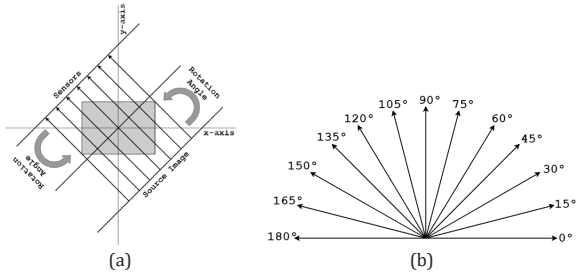

Fig. 2. Illustrating the radon transform theory: (a) generation of radon spectrum, (b) different angular directions considered for the present work to compute the line integral

Multi-resolution analysis. The time-frequency response of a signal (for present work it is an image) is represented through wavelet transform. Daubechies wavelets [22], which belongs to the family of discrete wavelet techniques, are used for the present work. Wavelets are used for multi-resolution analysis and their advantage includes: computational ease with minimum resource and time requirements. These orthogonal wavelets are characterized by maximum number of vanishing moments for some given support. We decompose an image into different frequencies with different resolutions for further analysis. The family of Daubechies wavelet is denoted as '*dbN*', where the wavelet family is denoted by the term '*db*' and the number of vanishing moments is represented by '*N*'. An image can be represented by the combination of different components of different coefficients. For the present work, the wavelet decomposition has been done at level 1 for *db1*, *db2* and *db3* which capture the constant, linear and quadratic coefficients of an image component. Four sub-band images namely, approximation coefficients (*cA*), horizontal coefficients (*cH*), vertical coefficients (*cV*), and diagonal coefficients (*cD*) are generated by this process for each of the *db1*, *db2* and *db3* part, resulting a total of 12 sub-band images.

Design of the descriptor. The image descriptor is developed by combining the idea of radon transform over multi-resolution analysis. The texture pattern of benign and malignant masses are different. The malignant mass region has more irregular in comparison to benign masses whose boundary regions are more re-

gular in shape. Radon transform computes the line integral of a set of pixels over a specified direction. So, if we compute radon transform on benign and malignant masses the line integral value will be different for each case. Figure 3 shows the radon spectrum of benign and malignant masses: Figure 3(a) is a benign mass and its radon spectrum is shown in Figure 3(c); Figure 3(b) is a malignant mass and its radon spectrum is shown in Figure 3(d).

There are several methods available for image decomposition like, divide by "n" and quad-tree decomposition among others. Here, we chose wavelet, as different directional approximation can be done through wavelet decomposition. From each of the sub-band images i.e. on *cA*, *cH*, *cV* and *cD*, we compute the radon spectrum. Finally, statistical values are computed from those radon-wavelet spectrum which are used to construct the feature vector.

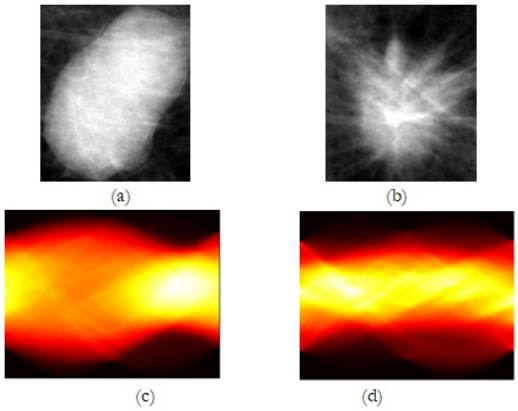

Fig. 3. ROI extracted from mammogram images and their radon spectrum (a) benign mass, (b) malignant mass, (c) radon spectrum of figure a, (a) radon spectrum of figure b

Feature vector generation.

In what follows, we summarize the generation of feature vector:

First, ROIs were extracted from the original mammogram images and contrast enhancement was done on each ROI. The enhanced ROI was then stored as a gray-scale image.

Wavelet decomposition at level 1 was done using Daubechies method for *db1*, *db2* and *db3*. This step generates 04 sub band images for each coefficients resulting a total of 12 sub-band images.

Radon transform is applied on the original ROI image and each of the 12 sub-band images generated on the previous step. At this step we generate a total of 13 radon spectrum.

From each of the 13 radon spectrum we compute one energy and three statistical features value. Altogether this step generates 52 features (04×13). Then, we compute 04 statistical features namely: entropy, mean, standard deviation and maximum coefficient of radon spectrum from the original gray-scale image too, so overall we get a feature vector of dimension 56 (52 + 04).

2.2. Classifiers

In our study, six different classifiers were used to train and classify the masses. They are Bayesian network (BN), Linear discriminant analysis (LDA), Logistic, Support vector machine (SVM), Multilayer perceptron (MLP) and Random Forest (RF). We compare the performance of these classifiers to find the best one. These classifiers are briefly explained below.

Bayesian network. For the Bayesian network (BN) we used K2, a hill-climbing technique which is a famous score-based algorithm that recovers the underlying distribution in the form of directed acyclic graph efficiently. Details can be found in [23].

Linear discriminant analysis. In linear discriminant analysis [24], we model the data as a set of multivariate normal distributions where a common covariance matrix exist with different mean vectors for different classes. LDA partition the feature-space by using a hyper-plane (HP), where two sides of the HP represent two classes. The class pattern is determined from the test dataset based on which side of the plane the classes lie.

Logistic. Logistic regression is used as a classification algorithm to assign observations to a discrete set of classes. The logistic classifier transforms its output using a logistic function (sigmoid) and returns a probability value. This probability value is then mapped into two or more classes [25].

Support vector machine. SVM classifies the data by constructing a hyper-plane (HP)on the high dimensional feature space. Different linear and non linear kernels can be used. For the present work, we used SVM tuned by a linear kernel since it's fast and presented promising results.

Multilayer perceptron. MLP is one of the most widely used classifiers. Here, the chosen configuration was *56-hl-2*, where 56 is the number of feature values, *hl* is the number of nodes in the hidden layer and 2 is the number of classes. *hl* can be determined empirically, by considering it as a function of the feature dimension (fifty six) and output classes (two). In our experiment the value of *hl* is considered as 29, i.e (56+2)/2.

Random forest. Theoretically, a random forest is defined as a collection of unpruned decision trees which are trained on bootstrap samples using random feature selection in the tree generation process. Among a large number of generated trees, each tree votes for a popular class and, by combining all, a decision is taken [26].

3. Experiments

3.1. Dataset & Pre-processing

A benchmark film mammography dataset known as BCDR-F03 [27,5] from the Breast Cancer Digital Repository, a wide-ranging public repository composed of Breast Cancer patients' cases from Portugal [6], was used in our experiment. The BCDR-F03 is one of the latest benchmarked film mammography dataset which

consists of 668 film mammogram images. Out of these 668 image there are 736 biopsy proven masses containing 426 benign masses and 310 malignant masses from 344 patients. Thus, in many cases a single image contains more than one masses.

For present work, we have considered one mass per image having a total of 668 masses. Out of these 668 masses, 662 images are considered for classification after removal of few extremely low resolution images. The samples provided are available in two different views namely carniocaudal (CC) and mediolateral oblique (MLO) view. In our data we have 328 CC views and 334 MLO views (almost equal ratio for fair comparison). Figure 4 shows different mammogram views with the lesions marked.

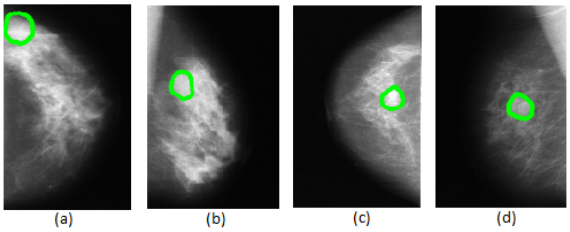

Fig. 4. Different mammogram views, (a) LCC, (b) LO, (c) RCC, (d) RO. The green boundary is the ROI

The pre-processing step includes (i) ROI extraction and (ii) contrast enhancement. ROI was extracted based on the information provided by the radiologist; an annotated file with the ROI coordinate information is provided along with the BCDR-F03 dataset. Using automated techniques ROIs were extracted and stored in separate folders based on different view types. Further, they were categorized into two class folders namely benign and malignant. Next, ROIs contrast enhancement was performed since original film mammograms are of very low contrast due to several factors (poor lighting condition, orientation, etc.); contrast is enhanced by subtracting the mean of the intensities in the image to each pixel. Figure 5 shows one original ROI and its contrast enhanced version.

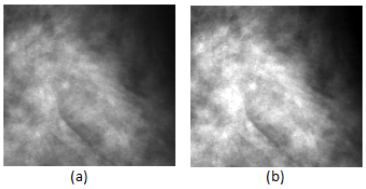

Fig. 5. Contrast enhancement, (a) original low contrast ROI, (b) contrast enhanced image

3.2. Evaluation Metrics

To measure the performance of the system, we use the Area Under the Curve of the Receiver Operator Characteristic (AUC). The ROC curve is created by plotting the true positive rate against the false positive rate. The AUC is a measure of discrimination also used in previous works on this dataset [6, 5], allowing then to make a comparison with our method.

3.3. Evaluation Strategy and System Configuration

We carried out three different type of tests: (i) mammogram mass classification from CC view, (ii) mammogram mass classification from MLO view and (iii) mammogram mass classification with both views combined. In each case, the dataset was divided into 60:40 ratio (60% data for training and rest 40% for testing), following the split of previous works for fair comparison [6, 4, 5].

Regarding the resources, all experiments were carried out using MATLAB 2017b software in a system with 2.8 GHz CPU, 8 GB RAM, 4 GB NVIDIA GPU.

3.4. Results and Analysis

In the present work, we not only propose a novel image descriptor for mammogram mass classification but also study the performance of different classifiers. In addition, the analysis of which image view is better for mass classification is also done. Table 1 shows the performance of six different classifiers (BN, LDA, Logistic, SVM, MLP and RF) for three different mammogram views: CC, MLO and both combined (best values are presented in bold face). From the first column of the table, which shows the output of the CC view, LDA and RF perform best with 0.986 AUC among the six classifiers. For the MLO view, RF shows the highest AUC of 0.738 and when both the views are combined (i.e. all images of CC and MLO are considered together) RF also shows highest AUC of 0.838. Given these results, it is possible conclude that RF is the best performer irrespective of image view.

Previous relevant work – analogy. Prior to this study, Moura et. al [6] proposed one histogram based image descriptor known as HGD and tested the method on the BCDR-F01 dataset, which is a subset of the BCDR-F03. They reported the highest AUC of 0.787 by HDG and 0.770 by traditional HOG. Nonetheless, these results are not solely based on image descriptor as clinical information was also used. Recently, Arevalo et. al [4, 5] proposed a deep learning based approach on BCDR-F03 dataset. Applying a convolution neural network (CNN) they obtained a AUC of 0.822; then, using CNN combined with the hand-crafted HGD features, the overall AUC was boosted upto 0.826, showing an improvement of 0.40%. Nonetheless, these two works are not comparable in true sense as different experimental framework were considered, i.e. for [6], a 80:20 data split for training and testing was considered while for [4, 5] the split was 60:40.

Table 2 shows the results reported and allows a qualitative comparison to our method (based on the present experimental consideration and framework). The proposed image descriptor performs significantly well without any clinical information as compared to the traditional approaches, thus proving the effectiveness of the image descriptor for mass classification.

Choosing the best classifier. Not only design of the descriptor, in this paper we also compare the performance of different classifiers to choose the best

Tab. 1. Mammogram mass classification results for CC, MLO and combined (CC+MLO) views on test dataset measured in AUC

Classifier	CC	MLO	CC+MLO
Baysian Network (BN)	0.934	0.690	0.816
Linear Discriminant Analaysis (LDA)	**0.986**	0.672	0.807
Logistic	0.958	0.674	0.811
Support Vector Machine (SVM)	0.977	0.682	0.783
Multilayer Perceptron (MLP)	0.985	0.618	0.813
Random Forest (RF)	**0.986**	**0.738**	**0.838**

Tab. 2. Performance comparison of proposed technique with baseline results (CC+MLO views combined)

Methods		AUC
Hand-crafted techniques [6]	HOG	0.770
	HGD	0.787
Deep-learning based approach [4] [5]	CNN	0.822
Deep learning + Hand-crafted techniques [5]	CNN + HDG	0.826
Proposed Method	Radon-wavelet based descriptor	**0.838**

one and a quantitative comparison is provided. Six different classifiers namely: Bayesian network (BN), Linear discriminant analysis (LDA), Logistic, Support vector machine (SVM), Multilayer perceptron (MLP) and Random Forest (RF) are considered for performance comparison. From Table 1 we can see Random Forest is the best performer among the six classifiers irrespective of the image view considered. For CC view images both the Random Forest and Linear Discriminant Analysis classifiers show an AUC of 0.986 followed by Multilayer Perceptron, Support Vector Machine and Logistic classifiers. We found, for CC view images, among the six classifiers except Baysian Network rests five provides almost neck to neck results. The CC view accuracy provided by Baysian Network is almost 5.27% less compared to the highest performer i.e. Random Forest. For MLO view, Random Forest shows an AUC of 0.738 which is highest among the six. Finally, when we combined both the views and considered all the images together then we found an AUC of 0.838 by the Random Forest classifier. Other four classifiers namely Multilayer Perceptron, Baysian Network, Linear Discriminant Analysis and Logistic also shows comparable performance. In this scenario, only Support vector Machine shows a bit less performance compared to all. Figure 6 shows a graphical representation of the performance comparison of different classifiers for different views.

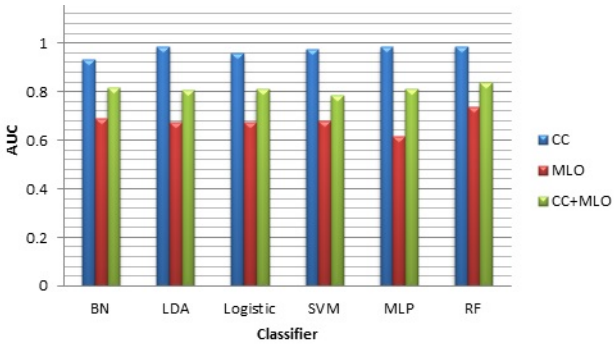

Fig. 6. Performance comparison of different classifiers for different image views

4. Conclusion

This paper provides a novel image descriptor which is based on radon transform and wavelet transform to seperate malignant and benign masses from film mammogram images. No doubt, automated diagnostics of breast cancer from mammogram images will support the radiologists by double checking their observations. Several methods are proposed in the literature for mammogram mass classifications from film mammogram images, but most of the time these descriptors show promising performance if combined with clinical information. In the present work, we propose a novel image descriptor which performs well without clinical information. The proposed image descriptor along with the random forest classifier shows an AUC of 0.986 for CC view, 0.738 for MLO view and 0.838 for the combined view. For mammogram mass classification the CC view is more effective than MLO one. In this experiment, we found that, CC view shows a 33.60% improvement over MLO.

To support the conclusions drawn on this work, namely the superiority of the image descriptor and the different discriminating powers of the CC and MLO views, our plan for future work includes evaluating the performance of the proposed descriptor on other publicly available film mammogram datasets and performing a statistical analysis over the results. Performance comparison of different classifier has been carried out in this paper. In future we intend to do performance analysis of more classifiers and performing statistical significance test on them is also in our plan.

AUTHORS

Sk Md Obaidullah* – Department of Informatics, University of Évora, Rua Romão Ramalho, 59, 7000-671 Évora, Portugal, e-mail: sk.obaidullah@gmail.com.
Sajib Ahmed – Department of Informatics, University of Évora, Rua Romão Ramalho, 59, 7000-671 Évora, Portugal, e-mail: jack6148@gmail.com.
Teresa Gonçalves – Department of Informatics, University of Évora, Rua Romão Ramalho, 59, 7000-671 Évora, Portugal, e-mail: tcg@uevora.pt.
Luís Rato – Department of Informatics, University of Évora, Rua Romão Ramalho, 59, 7000-671 Évora, Portugal, e-mail: lmr@uevora.pt.

*Corresponding author

REFERENCES

[1] "WHO, breast cancer". http://www.who.int/cancer/prevention/diagnosis-screening/breast-cancer/en/, 2018. Accessed on: 2020-09-20.

[2] P. Skaane, S. Hofvind, and A. Skjennald, "Randomized trial of screen-film versus full-field digital mammography with soft-copy reading in population-based screening program: follow-up and final results of Oslo II study", *Radiology*, vol. 244, no. 3, 2007, 708–717, 10.1148/radiol.2443061478.

[3] E. D. Pisano, R. E. Hendrick, M. J. Yaffe, J. K. Baum, S. Acharyya, J. B. Cormack, L. A. Hanna, E. F. Conant, L. L. Fajardo, L. W. Bassett, C. J. D'Orsi, R. A. Jong, M. Rebner, A. N. A. Tosteson, and C. A. Gatsonis, "Diagnostic Accuracy of Digital versus Film Mammography: Exploratory Analysis of Selected Population Subgroups in DMIST", *Radiology*, vol. 246, no. 2, 2008, 376–383, 10.1148/radiol.2461070200.

[4] J. Arevalo, F. A. González, R. Ramos-Pollán, J. L. Oliveira, and M. A. Guevara Lopez, "Convolutional neural networks for mammography mass lesion classification". In: *2015 37th Annual International Conference of the IEEE Engineering in Medicine and Biology Society (EMBC)*, 2015, 797–800, 10.1109/EMBC.2015.7318482, ISSN: 1558-4615.

[5] J. Arevalo, F. A. González, R. Ramos-Pollán, J. L. Oliveira, and M. A. Guevara Lopez, "Representation learning for mammography mass lesion classification with convolutional neural networks", *Computer Methods and Programs in Biomedicine*, vol. 127, 2016, 248–257, 10.1016/j.cmpb.2015.12.014.

[6] D. C. Moura and M. A. Guevara López, "An evaluation of image descriptors combined with clinical data for breast cancer diagnosis", *International Journal of Computer Assisted Radiology and Surgery*, vol. 8, no. 4, 2013, 561–574, 10.1007/s11548-013-0838-2.

[7] A. S. Constantinidis, M. C. Fairhurst, and A. F. R. Rahman, "A new multi-expert decision combination algorithm and its application to the detection of circumscribed masses in digital mammograms", *Pattern Recognition*, vol. 34, no. 8, 2001, 1527–1537, 10.1016/S0031-3203(00)00088-1.

[8] S. O. Belkasim, M. Shridhar, and M. Ahmadi, "Pattern recognition with moment invariants: A comparative study and new results", *Pattern Recognition*, vol. 24, no. 12, 1991, 1117–1138, 10.1016/0031-3203(91)90140-Z.

[9] R. M. Haralick, K. Shanmugam, and I. Dinstein, "Textural Features for Image Classification", *IEEE Transactions on Systems, Man, and Cybernetics*, vol. SMC-3, no. 6, 1973, 610–621, 10.1109/TSMC.1973.4309314, Conference Name: IEEE Transactions on Systems, Man, and Cybernetics.

[10] S. Yu and L. Guan, "A CAD system for the automatic detection of clustered microcalcifications in digitized mammogram films", *IEEE transactions on medical imaging*, vol. 19, no. 2, 2000, 115–126, 10.1109/42.836371.

[11] A. Dhawan, Y. Chitre, and C. Kaiser-Bonasso, "Analysis of mammographic microcalcifications using gray-level image structure features", *IEEE Transactions on Medical Imaging*, vol. 15, no. 3, 1996, 246–259, 10.1109/42.500063, Conference Name: IEEE Transactions on Medical Imaging.

[12] D. Wang, L. Shi, and P. Ann Heng, "Automatic detection of breast cancers in mammograms using structured support vector machines", *Neurocomputing*, vol. 72, no. 13, 2009, 3296–3302, 10.1016/j.neucom.2009.02.015.

[13] S. Dua, H. Singh, and H. W. Thompson, "Associative classification of mammograms using weighted rules", *Expert Systems with Applications*, vol. 36, no. 5, 2009, 9250–9259, 10.1016/j.eswa.2008.12.050.

[14] B. Sahiner, H.-P. Chan, N. Petrick, M. A. Helvie, and L. M. Hadjiiski, "Improvement of mammographic mass characterization using spiculation measures and morphological features", *Medical Physics*, vol. 28, no. 7, 2001, 1455–1465, 10.1118/1.1381548.

[15] C. Mazo, E. Alegre, M. Trujillo, and V. González-Castro, "Tissues Classification of the Cardiovascular System Using Texture Descriptors". In: M. Valdés Hernández and V. González-Castro, eds., *Medical Image Understanding and Analysis*, Cham, 2017, 123–132, 10.1007/978-3-319-60964-5_11.

[16] A. O'Neil, M. Shepherd, E. Beveridge, and K. Goatman. "A Comparison of Texture Features Versus Deep Learning for Image Classification in Interstitial Lung Disease". In: M. Valdés Hernández

and V. González-Castro, eds., *Medical Image Understanding and Analysis*, volume 723, 743–753. Springer International Publishing, Cham, 2017.

[17] C. B. R. Ferreira and D. L. Borges, "Analysis of mammogram classification using a wavelet transform decomposition", *Pattern Recognition Letters*, vol. 24, no. 7, 2003, 973–982, 10.1016/S0167-8655(02)00221-0.

[18] E. A. Rashed, I. A. Ismail, and S. I. Zaki, "Multiresolution mammogram analysis in multilevel decomposition", *Pattern Recognition Letters*, vol. 28, no. 2, 2007, 286–292, 10.1016/j.patrec.2006.07.010.

[19] M. Meselhy Eltoukhy, I. Faye, and B. Belhaouari Samir, "A comparison of wavelet and curvelet for breast cancer diagnosis in digital mammogram", *Computers in Biology and Medicine*, vol. 40, no. 4, 2010, 384–391, 10.1016/j.compbiomed.2010.02.002.

[20] R. Ramos-Pollán, M. A. Guevara-López, C. Suárez-Ortega, G. Díaz-Herrero, J. M. Franco-Valiente, M. Rubio-Del-Solar, N. González-de Posada, M. A. P. Vaz, J. Loureiro, and I. Ramos, "Discovering mammography-based machine learning classifiers for breast cancer diagnosis", *Journal of Medical Systems*, vol. 36, no. 4, 2012, 2259–2269, 10.1007/s10916-011-9693-2.

[21] S. R. Deans, *The Radon transform and some of its applications*, Wiley: New York, 1983.

[22] S. Mallat, "A theory for multiresolution signal decomposition: the wavelet representation", *IEEE Transactions on Pattern Analysis and Machine Intelligence*, vol. 11, no. 7, 1989, 674–693, 10.1109/34.192463, Conference Name: IEEE Transactions on Pattern Analysis and Machine Intelligence.

[23] C. Bielza, G. Li, and P. Larrañaga, "Multidimensional classification with Bayesian networks", *International Journal of Approximate Reasoning*, vol. 52, no. 6, 2011, 705–727, 10.1016/j.ijar.2011.01.007.

[24] S. Mika, G. Ratsch, J. Weston, B. Scholkopf, and K. Mullers, "Fisher discriminant analysis with kernels". In: *Neural Networks for Signal Processing IX: Proceedings of the 1999 IEEE Signal Processing Society Workshop*, 1999, 41–48, 10.1109/NNSP.1999.788121.

[25] "Logistic Regression - ML Glossary documentation". https://ml-cheatsheet.readthedocs.io/en/latest/logistic_regression.html, 2017. Accessed on: 2020-09-20.

[26] K. C. Santosh and S. Antani, "Automated Chest X-Ray Screening: Can Lung Region Symmetry Help Detect Pulmonary Abnormalities?", *IEEE transactions on medical imaging*, vol. 37, no. 5, 2018, 1168–1177, 10.1109/TMI.2017.2775636.

[27] "Breast Cancer Digital Repository". https://bcdr.eu/information/about. Accessed on: 2020-09-25.